Monthly Notices of the ROYAL ASTRONOMICAL SOCIETY

MNRAS **522,** L51–L55 (2023) https://doi.org/10.1093/mnrasl/slad027

Confirmation and Keplerian motion of the gap-carving protoplanet HD 169142 b

Iain Hammond [1,2★] Valentin Christiaens [2] Daniel J. Price [1] Claudia Toci [3] Christophe Pinte [1,4] Sandrine Juillard[2] and Himanshi Garg [1]

[1] *School of Physics and Astronomy, Monash University, Vic 3800, Australia*
[2] *Space Sciences, Technologies and Astrophysics Research (STAR) Institute, Université de Liège, Allée du Six Août 19c, B-4000 Sart Tilman, Belgium*
[3] *European Southern Observatory (ESO), Karl-Schwarzschild-Str 2, D-85748 Garching, Germany*
[4] *Université Grenoble Alpes, CNRS, IPAG, F-38000 Grenoble, France*

Accepted 2023 February 20. Received 2023 February 20; in original form 2022 December 7

ABSTRACT

We present the re-detection of a compact source in the face-on protoplanetary disc surrounding HD 169142, using VLT/SPHERE data in *YJH* bands. The source is found at a separation of 0.″319 (∼37 au) from the star. Three lines of evidence argue in favour of the signal tracing a protoplanet: (i) it is found in the annular gap separating the two bright rings of the disc, as predicted by theory; (ii) it is moving at the expected Keplerian velocity for an object at ∼37 au in the 2015, 2017, and 2019 data sets; and (iii) we also detect a spiral-shaped signal whose morphology is consistent with the expected outer spiral wake triggered by a planet in the gap, based on dedicated hydrodynamical simulations of the system. The *YJH* colours we extracted for the object are consistent with tracing scattered starlight, suggesting that the protoplanet is enshrouded in a significant amount of dust, as expected for a circumplanetary disc or envelope surrounding a gap-clearing Jovian-mass protoplanet.

Key words: protoplanetary discs – planet–disc interactions – stars: individual: HD 169142.

1 INTRODUCTION

The lack of a statistically significant number of unambiguous protoplanet detections limits our understanding of giant planet formation. The protoplanetary disc of HD 169142 is a prime location to search for and expand the sample of directly imaged protoplanets. HD 169142 is a nearby (114.8 pc, Gaia Collaboration et al. 2022), 6-Myr-old, 1.85$M_\odot$ (Gratton et al. 2019; hereafter G19) Herbig Ae star surrounded by a protoplanetary disc seen almost face-on (i = 13°, PA = 5°; Raman et al. 2006). Observations have revealed two sets of rings at 25 and 60 au delimit a 22-au radius central cavity and an annular gap at 38 au, both depleted in dust and gas (Honda et al. 2012; Quanz et al. 2013; Fedele et al. 2017; Macías et al. 2017, 2019; Pohl et al. 2017; Pérez et al. 2019; Garg et al. 2022). Dedicated hydrodynamical simulations suggest the presence of two 2–4 M_J planets, in the cavity and gap, respectively (Toci et al. 2020).

Protoplanet candidate detections were first claimed around HD 169142 based on high-contrast VLT/NACO L'-band and MagAO near-IR observations (Biller et al. 2014; Reggiani et al. 2014). Polarimetric differential imaging (PDI, Kuhn, Potter & Parise 2001) observations with the Spectro-Polarimetic High contrast imager for Exo-planets REsearch (SPHERE; Beuzit et al. 2008) have also revealed a planet candidate in the disc's annular gap at ∼36 au separation. Pohl et al. (2017) presented J-band PDI of HD 169142 at λ_c = 1.24 μm. Although not discussed at the time, our reduction of this data shows scattered light emission in the annular gap, suggestive of a localized collection of dust at a position angle of ∼44°. Bertrang et al. (2018) presented a tentative re-detection in SPHERE/ZIMPOL data at shorter wavelengths although this feature was not mentioned either. Based on SPHERE/IFS data, Ligi et al. (2018) suggested that the L' protoplanet candidates from 2014 are tracing filtered signals from the bright inner ring, while also presenting a bright structure at 93 mas interior to the inner ring. G19 claimed the first possible detection of the outer planet in the annular gap using SPHERE/IRDIFS observations (their 'blob D'). However, several observations used in their work reached insufficient contrast for a firm re-detection of their candidate, due to a combination of sub-optimal observing conditions, short integration time, and aggressive post-processing. Their candidate was later found to overlap with a non-Keplerian kinematic feature (Garg et al. 2022). In this Letter, we present the re-detection of the compact source in the gap between the two dust rings at three epochs, as well as the first detection of its outer spiral wake, by re-reducing archival SPHERE/VLT data with state-of-the-art point-spread-function subtraction techniques. We show source movement over the 4 yr between observations consistent with Keplerian orbital motion.

2 OBSERVATIONS AND DATA REDUCTION

Pohl et al. (2017) first published the 2015 data, employing PDI. The `N_ALC_YJ_S` coronagraph was used to attenuate light from the star, allowing for 32 s exposures in J-band. A total of five polarimetric cycles were captured, each consisting of four datacubes in the four Stokes parameters. We re-reduced this data set using the IRDIS Data reduction for Accurate Polarimetry pipeline (IRDAP 1.3.4, van

★ E-mail: iain.hammond@monash.edu

Table 1. Summary of the archival VLT/SPHERE high-contrast imaging observations of HD 169142 used in this work.

Date	Strategy	Program	Instrument	Filter	Plate scale[(a)] [mas px^{-1}]	Coronagraph	DIT [s]	T_{int}[(b)] [min]	$<\beta>$ [(c)] ["]	ΔPA[(d)] [°]	SNR_b[(e)]
2015 May 03	PDI	095.C-0273(A)	IRDIS	*J*	12.263 ± 0.009	N_ALC_YJ_S	32	53.3	0.44	–	–
2015 June 28	ASDI	095.C-0298(C)	IFS	*YJH*	7.46 ± 0.02	N_ALC_YJH_S	64	58.7	1.00	35.0	4.0
2017 Apr 30	ASDI	198.C-0209(G)	IFS	*YJH*	7.46 ± 0.02	–	2	38.4	0.62	97.8	4.3
2019 May 19[(f)]	ASDI	1100.C-0481(N)	IFS	*YJH*	7.46 ± 0.02	N_ALC_Ks	96	76.8	0.59	118.2	4.5
2019 May 19[(f)]	ADI	1100.C-0481(N)	IRDIS	*K12*	12.265 ± 0.009	N_ALC_Ks	96	76.8	0.59	118.2	–

Note: [(a)]Maire et al. (2016). [(b)]Total integration time after bad frame removal. [(c)]Average seeing at $\lambda = 500$nm. [(d)]Parallactic angle variation. [(e)]Signal-to-noise ratio of the protoplanet achieved in the processed image, following the definition in Mawet et al. (2014). [(f)] New to this work.

Holstein et al. 2020) with default parameters to produce a Q_ϕ image. We interpolated the star position using the centre calibration files from the start and end of the observation.

We re-reduced SPHERE observations of HD 169142 obtained in `IRDIFS-EXT` mode, corresponding to simultaneous acquisition of Integral Field Spectrograph (IFS, Claudi et al. 2008) images in the *YJH*-bands and IRDIS images with the K1 and K2 filters ($\lambda \approx$ 2.11 and 2.25 μm, respectively). These are summarized in Table 1. Our selection was motivated by needing long integration times and large bandwidth. The 2015 and 2017 data sets were published in Ligi et al. (2018), while the 2019 data is new to this work. We only considered the 2019 epoch of SPHERE/IRDIS *K12* data, as it corresponded to the best observing conditions and integration time. We reduced both IFS and IRDIS data using an in-house pipeline, VCAL-SPHERE[1] (Christiaens et al. 2021). The pipeline uses the ESO Recipe Execution Tool ESOREX (v3.13.6) for calibration, whereas for pre- and post-processing we used the Vortex Image Processing package (VIP; Gomez Gonzalez et al. 2017; Christiaens et al., JOSS, submitted). For IRDIS, our pipeline involved: (i) flat-fielding, (ii) principal component analysis (PCA, Amara & Quanz 2012)-based sky subtraction, (iii) bad pixel correction, (iv) centring of the coronagraphic images via satellite spots, (v) centring of the non-coronagraphic unsaturated PSF images using 2D Gaussian fits, (vi) anamorphism correction, (vii) fine centring and bad frame removal using a bright background star, (viii) final PSF creation, and (ix) post-processing with median-angular differential imaging (ADI; Marois et al. 2006), PCA-ADI in full-frame and annular PCA-ADI. The final *K*1 and *K*2 images are combined to further enhance the SNR of faint circumstellar signals (hereafter, referred to as *K12* image). Reduction of the IFS data involved additional steps compared to IRDIS: master darks, master detector and instrument flats, sky cubes, spectra positions, and wavelength calibration were computed to produce calibrated spectral cubes of 39 channels. VIP functions handled pre-processing as for our IRDIS data (see above). Our pipeline then leveraged both angular and spectral differential imaging (SDI) using PCA (i.e. PCA-ASDI) for an optimal subtraction of speckles, through the corresponding routines of VIP. We used annular PCA-ASDI in two steps (SDI + ADI) on the 2015 and 2017 data sets, as they were acquired in mediocre observing conditions, and in a single step for the 2019 data set (see details on each PCA-ASDI flavour in Christiaens et al. 2019). These choices led to the best-achieved contrasts, respectively. We explored 1–20 principal components.

[1]https://github.com/VChristiaens/vcal_sphere

3 RESULTS

3.1 Compact source in the annular gap

Fig. 1 shows our new reduction of the PDI data set (left-hand panel) alongside our re-detection of both the compact source in the gap and the first detection of spiral-shaped signal in its wake in the 2017 and 2019 IFS data sets. The ASDI reduction of the 2015 IFS data set, of lower quality, is provided in Appendix A. The source is robust to the number of principal components (1–20) and has an optimal SNR of ∼4.0, ∼4.3, and ∼4.5 in the 2015, 2017, and 2019 IFS data sets, respectively, after considering small number statistics (Mawet et al. 2014). We consider these values as lower limits for the 2017 and 2019 data given the presence of a negative ADI-induced spiral signature (associated with a true disc feature also seen in PDI images; Section 3.2) overlapping with noise apertures. Given that the signal is located within the cleared annular gap, it does not trace filtered ring signal.

We measured the position of the compact source to be $r = 0''.319 \pm 0''.013$ and PA $= 33.9 \pm 2.3°$ in the 2019 IFS data set. We used the negative fake companion technique (NEGFC; Lagrange et al. 2010) combined with PCA-ADI applied to each spectral channel, before median-combining the residuals along the wavelength axis. We first used a Nelder–Mead simplex algorithm to obtain a guess on the (negative) planet flux and location, which minimized pixel intensities in the vicinity of the planet. We then fed this estimate to a Markov chain Monte Carlo algorithm to determine the posterior probability distribution of the three parameters after 2500 steps (30 per cent burn-in). A new expression for the log-probability function was used to account for residual speckle uncertainty on the parameters (Christiaens et al. 2021). As HD 169142 rotates fast on the sky when viewed from Cerro Paranal, we also considered a 1.2° uncertainty associated to the average smearing over the sequence in 96-s long exposures.

For the PDI data and remaining IFS data sets (where the protoplanet could only be imaged through ASDI) we performed a 2D Gaussian fit to the source. We derived $r = 0''.321 \pm 0.010$ and PA $= 43.7 \pm 1.7°$ in the PDI image. For the IFS data sets, we derived $r = 0''.0.319 \pm 0.011$ and PA $= 44.1 \pm 2.3°$ for 2015 and $r = 0''.313 \pm 0.006$ and $39.8 \pm 2.3°$ for 2017 (i.e. in agreement with the values reported in G19). For all data sets, the final quoted uncertainties were found by summing the error on our fits with all sources of systematic error in quadrature, including those associated to star centring (∼5 mas) and to the true north of IFS and IRDIS (Maire et al. 2016). Considering a distance of 114.8 ± 0.4 pc, disc PA = 5°, and inclination $i = 13°$, the deprojected physical separation of the source in our IFS data is 37.2 ± 1.5 au. Fig. 2 shows that our four PA measurements are consistent with the predicted Keplerian motion for a planet at 37 au orbiting a $1.85 M_\odot$ star.

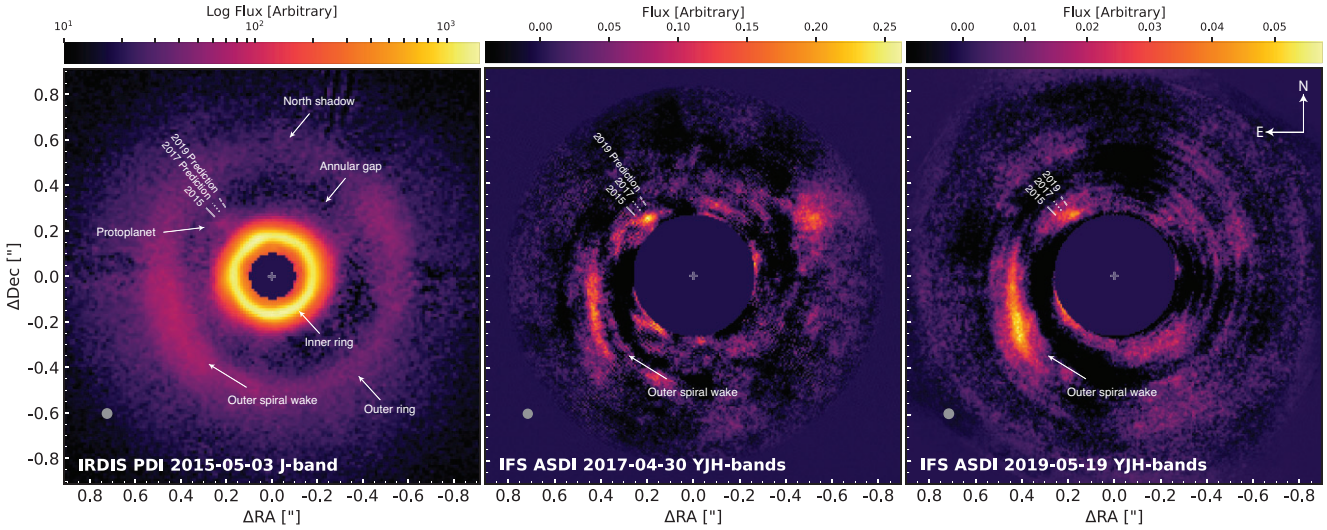

Figure 1. SPHERE near-infrared observations of the disc surrounding HD 169142. Left-hand panel: IRDIS PDI data tracing light scattered off small grains, showcasing a concentration of grains in two rings and a localized collection of dust in the annular gap, suggestive of circumplanetary material. The inner working angle of the coronagraph has been masked. Middle- and right-hand panel: Detection of the protoplanet and accompanying outer spiral wake with SPHERE/IFS. The bright inner disc has been masked. In each image, the grey patch represents the FWHM of the non-coronagraphic images obtained during the observing sequence.

3.2 Disc features

Rings are most obvious in the Q_ϕ image (see left-hand panel of Fig. 1 where we have labelled key disc features). We recover the compact signal at the same location as presented in Pohl et al. (2017) in the region with excess scattering between the two dust rings (left-hand panel). Brightness variations in azimuth can be seen on the outer ring: there is an emission deficit to the north and overbrightness to the east. Our ASDI images obtained in the best observing conditions (Fig. 1) reveal a spiral arm to the east. The emission coincides with the overbrightness in the outer ring seen in scattered light (left-hand panel), suggesting an unresolved superposition of the spiral arm and the outer dust ring. The overall signal morphology in our images suggests emission from a protoplanet connected to a trailing spiral arm to the east, which would imply clockwise rotation.

3.3 Spectrum of the compact source

Given the faintness of the compact source, we created three sub-cubes from a weighted average along the wavelength axis of the 4D IFS cube, following the IRDIS *Y*, *J*, and *H*2 filter transmission curves, respectively. Fig. 3 shows that the compact source is re-detected separately in each filter. We did not re-detect any compact signal in the IRDIS *K12* images, however, the spiral was recovered. Each cube was post-processed using PCA-ADI in a single annulus encompassing the same radial separation as the protoplanet, using the same rotation threshold and annulus width as in Section 2. We set the number of principal components to maximize the SNR of the protoplanet using the definition in Mawet et al. (2014).

Fig. 3 shows the contrast spectrum for the source. We measured the flux in each band using the NEGFC technique as in Section 3.1. We derive a contrast with respect to the star of $1.49 \times 10^{-5} \pm 5.95 \times 10^{-6}$, $1.72 \times 10^{-5} \pm 6.16 \times 10^{-6}$, and $1.93 \times 10^{-5} \pm 1.17 \times 10^{-5}$ for the *Y*, *J*, and *H2* bands, respectively. Non-detection in the K12 band gives a 3σ upper contrast limit of 5.1×10^{-5}.

4 DISCUSSION

The motion of the source matches the expectations for a protoplanet on a circular orbit at a radius of 37 au around a 1.85 $M_\odot$ star (Fig. 2). Uncertainties (for which we included systematic errors) cannot account for such displacement over 4 yr. Clockwise rotation is consistent with previous studies of the motion of disc substructures using multi-epoch imaging (e.g. Ligi et al. 2018, G19). The compact source coincides with a localized kinematic excess with respect to Keplerian rotation in the gap (Garg et al. 2022), suggesting an embedded planet.

The depleted annular gap has been explained by the presence of a (super-) Jupiter mass planet (Fedele et al. 2017; Bae, Pinilla & Birnstiel 2018; Lodato et al. 2019; Toci et al. 2020), where 6 Myr have provided time for a planet to deplete the gap of dust grains. ALMA observations at 1.3 mm (Pérez et al. 2019) suggest that these grains have been most strongly filtered from the annular gap as expected for planet-induced clearing (Rice et al. 2006), whereas smaller grains remain coupled to the gas close to the protoplanet as seen in Fig. 1 (left-hand panel). Each tracer has a different radial extent (i.e. smaller gap in sub-mm, larger in mm), which is expected for different grain sizes in the case of clearing by a planet (Pinilla, Benisty & Birnstiel 2012). As the gap is depleted in gas (but not entirely) we can rule out dead zone dust filtration or photoevaporation. Furthermore, the rings do not correspond to snowlines of gas volatiles (Macías et al. 2019).

The presence of a planet also accounts for the spiral arm observed to the east, as suggested by hydrodynamical simulations and analytical wake models (Toci et al. 2020; Garg et al. 2022; Poblete et al. 2022). Thermal emission from the edge of the outer ring can be rejected as (i) the spiral has a non-zero pitch angle (not consistent with a ring) and (ii) is limited in azimuthal extent. Such a feature does not appear elsewhere in the disc. We do not resolve the inner wake, which is likely overlapping with the bright inner ring, although the 2011 *H*-band Subaru/HiCIAO image of the system shows a tentative extended signal in the annular gap at the expected location of the inner spiral wake (towards north and north-east; Momose et al. 2015). We note a reduction in surface brightness of the outer ring towards

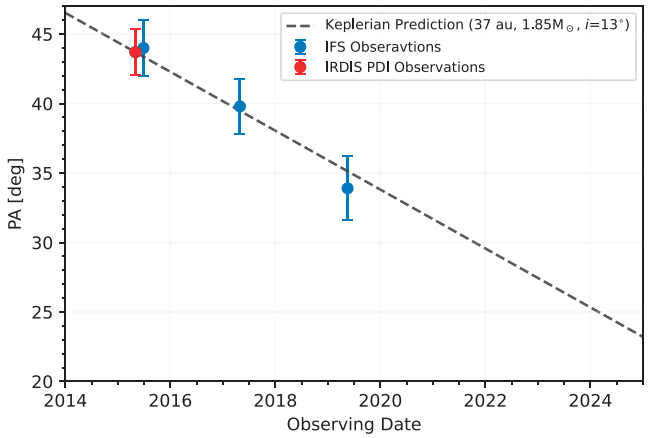

Figure 2. Measured position angle of the protoplanet in the IFS and PDI data sets (blue and red error bars, respectively), compared to expected Keplerian rotation around a 1.85$M_\odot$ star for an object at 37 au on an orbit inclined by 13° to the plane of the sky (dashed line).

PA $\sim -15°$–$30°$ (also seen in *R'*, *I'*, *H*, and *J*-band irrespective of instrument, Momose et al. 2015; Monnier et al. 2017; Bertrang et al. 2018; Tschudi & Schmid 2021; Rich et al. 2022), which could be caused by shadowing from either the inner ring or the expected inner spiral wake.

Fig. 3 compares our contrast spectrum of HD 169142 b with the expected contrast spectrum for PDS 70 b and for circumplanetary disc (CPD) models presented in Szulágyi et al. (2019), obtained considering the SED of the star presented in Wagner et al. (2015). For PDS 70 b, we considered the best-fitting BT-SETTL model inferred in Wang et al. (2021). We used SPECIAL (Christiaens 2022) to apply the best-fitting value found for extinction ($A_V = 5.4$) and resample the model to the IFS spectral resolution. The non-detection of the protoplanet in the 2019 IRDIS K12 images suggests a $J - K12$ colour lower than 2.1 ± 0.4 mag. This implies that the colour of HD 169142 b is likely not as red as PDS 70 b ($J - K12 \approx 2.2$; Wang et al. 2021). The contrast spectrum is consistent with NIR SED predictions for CPD models of either 1 or 5 M_J (Szulágyi et al. 2019). The spectrum of forming giant planets and their CPD is expected to be dominated by scattered starlight if the planet is embedded, making them potentially detectable in Q_ϕ polarized maps for favourable (e.g. face-on) geometries (Szulágyi et al. 2019; Szulágyi & Garufi 2021). Our observations suggest this is the case and the protoplanet spectrum likely peaks far into the infrared due to extinction by the CPD or envelope. Such detection suggests that leveraging polarized light off a planet's circumplanetary dust may be a powerful way to reveal protoplanets in near face-on discs.

To show that our observations can be qualitatively explained in the protoplanet scenario, we compare the observed 2015 Q_ϕ image with a synthetic Q_ϕ image at 1.25 μm (Fig. 4) obtained by processing a snapshot (~400 orbits, 0.13 Myr of evolution) of the 3D hydrodynamical model presented in Toci et al. (2020) with radiative transfer code MCFOST (Pinte et al. 2006). We refer the reader to Toci et al. (2020) for details on the setup of the PHANTOM (Price et al. 2018) model. The comparison shows how the presence of a planet located at the detected position of our compact source can qualitatively explain both the annular gap and the spiral wake. The model includes two giant planets (M~2.5 M_J), one located in the inner cavity, at 17 au, and one located in between the two rings, at a PA of 44° to match the position of the observed compact source. While some emission due to the presence of small dust grains close to the planet can be seen

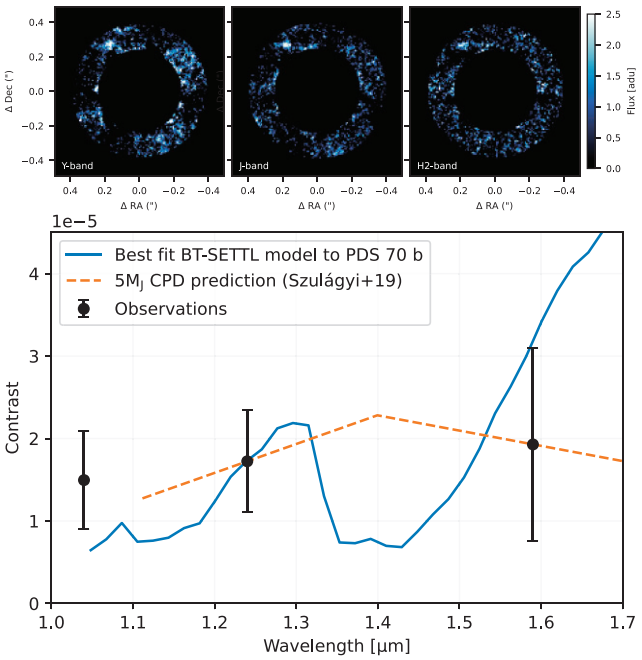

Figure 3. (Top) Detection of the protoplanet in individual *Y*, *J*, and *H*2-band images using annular PCA-ADI applied to the 2019 IFS data set. (bottom) Corresponding contrast of the planet with respect to the star (black error bars), compared to the expected contrast spectrum for the best-fitting BT-SETTL model of PDS 70 b (Wang et al. 2021) (blue curve) and for a circumplanetary disc model presented in Szulágyi et al. (2019; dashed curve).

in the model, one should not expect to fully recover the emission as circumplanetary material was excluded from the simulation. The comparison reveals some limitations of the model: the inner ring is slightly wider, implying that the inner planet should be located 1–2 au inward, and the darkness of the gap is not matched, suggesting either a larger disc aspect ratio or a flared disc (for a discussion, see Macías et al. 2019). We did not attempt to fine-tune these parameters, nor the planet masses and number of orbits, as fresh modelling of this source is beyond the scope of this work.

Observations with longer integration times are required to extract a higher signal-to-noise NIR spectrum of the protoplanet, and follow-up at mid-IR wavelengths may confirm the expected thermal excess of the CPD (Zhu 2015; Szulágyi et al. 2019). Deep ALMA sub-mm continuum images may re-detect the CPD, although the outer ring pressure bump may significantly limit the amount of large grains fed to the CPD. Given the amount of small dust surrounding the protoplanet, long-wavelength hydrogen recombination lines (e.g. Br-α) may be needed to confirm accretion on to the protoplanet. If most protoplanets are enshrouded in large amounts of dust as evidenced here, extinction may account for the lack of Hα detections in discs with strong planet signposts (e.g. Zurlo et al. 2020), except for the most favourable cases corresponding to deep and wide (e.g. multiplanet carved) gaps.

5 CONCLUSIONS

We confirm the protoplanet HD 169142 b first proposed in G19, inside an annular gap at 0.″319 using angular and SDI. The $10.2 \pm 2.8°$ shift in position angle between 2015 and 2019 with intermediate separation in 2017 is consistent with Keplerian motion of the planet. The clockwise motion is consistent with a trailing spiral arm observed to the east. Hydrodynamical simulations from Toci et al. (2020)

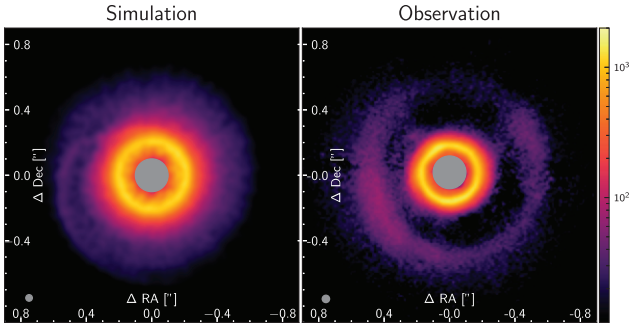

Figure 4. Comparison between the observations and the prediction from the Toci et al. (2020) models.

qualitatively reproduce the observed spiral wake associated with the planet. The contrast spectrum we extracted for the protoplanet suggests starlight scattered off circumplanetary dust, consistent with the detection in polarized intensity and expectations from CPD models in Szulágyi et al. (2019).

ACKNOWLEDGEMENTS

We thank Myriam Benisty and Roxanne Ligi for useful discussions. IH acknowledges a Research Training Program scholarship from the Australian Government. IH, DP, CP, and HG acknowledge the Australian Research Council funding via DP180104235. VC acknowledges a post-doctoral fellowship from the Belgian F.R.S.-FNRS. CT acknowledges the European Union's Horizon 2020 research and innovation programme, Marie Sklodowska Curie grant agreement number 823823 (DUSTBUSTERS RISE project). We made use of the Multi-modal Australian ScienceS Imaging and Visualization Environment (MASSIVE) (www.massive.org.au) and data from the European Space Agency (ESA) mission *Gaia*.

DATA AVAILABILITY

Data is available through Monash University's *Bridges* research repository via doi: 10.26180/22146428.

REFERENCES

Amara A., Quanz S. P., 2012, MNRAS, 427, 948
Bae J., Pinilla P., Birnstiel T., 2018, ApJ, 864, L26
Bertrang G. H. M., et al., 2018, MNRAS, 474, 5105
Beuzit J.-L. et al., 2008, in McLean I. S., Casali M. M., eds, SPIE Conf. Ser. Vol. 7014, Ground-based and Airborne Instrumentation for Astronomy II. SPIE, Washington, p. 701418
Biller B. A. et al., 2014, ApJ, 792, L22
Christiaens V., 2022, J. Open Source Soft., 7, 4456
Christiaens V. et al., 2019, MNRAS, 486, 5819
Christiaens V. et al., 2021, MNRAS, 502, 6117
Claudi R. U. et al., 2008, in McLean I. S., Casali M. M., eds, SPIE Conf. Ser. Vol. 7014, Ground-based and Airborne Instrumentation for Astronomy II. SPIE, Washington, p. 70143E
Fedele D. et al., 2017, A&A, 600, A72
Gaia Collaboration et al., 2022, preprint (arXiv:2208.00211)
Garg H. et al., 2022, MNRAS, 517, 5942
Gomez Gonzalez C. A. et al., 2017, AJ, 154, 7
Gratton R. et al., 2019, A&A, 623, A140
Honda M. et al., 2012, ApJ, 752, 143
Kuhn J. R., Potter D., Parise B., 2001, ApJ, 553, L189
Lagrange A. M. et al., 2010, Science, 329, 57
Ligi R. et al., 2018, MNRAS, 473, 1774
Lodato G. et al., 2019, MNRAS, 486, 453
Macías E., et al., 2017, ApJ, 838, 97
Macías E. et al., 2019, ApJ, 881, 159
Maire A.-L. et al., 2016, in Evans C. J. et al., eds, SPIE Conf. Ser. Vol. 9908, Ground-based and Airborne Instrumentation for Astronomy VI. SPIE, Washington, p. 990834
Marois C., et al., 2006, ApJ, 641, 556
Mawet D. et al., 2014, ApJ, 792, 97
Momose M. et al., 2015, PASJ, 67, 83
Monnier J. D. et al., 2017, ApJ, 838, 20
Pérez S., et al., 2019, AJ, 158, 15
Pinilla P., Benisty M., Birnstiel T., 2012, A&A, 545, A81
Pinte C., Ménard F., Duchêne G., Bastien P., 2006, A&A, 459, 797
Poblete P. P. et al., 2022, MNRAS, 510, 205
Pohl A. et al., 2017, ApJ, 850, 52
Price D. J. et al., 2018, PASA, 35, e031
Quanz S. P., et al., 2013, ApJ, 766, L2
Raman A., et al., 2006, AJ, 131, 2290
Reggiani M. et al., 2014, ApJ, 792, L23
Rice W. K. M., et al., 2006, MNRAS, 373, 1619
Rich E. A. et al., 2022, AJ, 164, 109
Szulágyi J., Garufi A., 2021, MNRAS, 506, 73
Szulágyi J., Dullemond C. P., Pohl A., Quanz S. P., 2019, MNRAS, 487, 1248
Toci C., Lodato G., Fedele D., Testi L., Pinte C., 2020, ApJ, 888, L4
Tschudi C., Schmid H. M., 2021, A&A, 655, A37
Wagner K. R. et al., 2015, ApJ, 798, 94
Wang J. J. et al., 2021, AJ, 161, 148
Zhu Z., 2015, ApJ, 799, 16
Zurlo A. et al., 2020, A&A, 633, A119
van Holstein R. G. et al., 2020, A&A, 633, A64

APPENDIX A: 2015 AND 2017 SPHERE/IFS DATA

Fig. A1 shows our reduction of the 2015 June 28 and 2017 April 30 SPHERE/IFS data sets, where we detect the compact emission from the protoplanet at a SNR∼4.0 and 4.3, respectively. The outer spiral wake is recovered in the 2017 data set (Fig. 1).

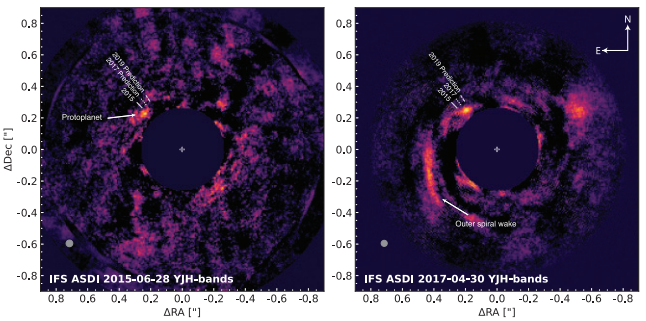

Figure A1. ASDI reductions for the 2015 and 2017 IFS data showcasing motion of the protoplanet. Solid, dotted, and dashed ticks indicate the position of the protoplanet in the 2015, 2017, and 2019 IFS data sets, respectively.

This paper has been typeset from a TEX/LATEX file prepared by the author.